



1 **NH₃ spatio-temporal variability over Paris, Mexico and Toronto and its link to**
2 **PM_{2.5} during pollution events**

3

4 Camille Viatte¹, Rimal Abeed¹, Shoma Yamanouchi^{2,3}, William Porter⁴, Sarah Safieddine¹, Martin Van
5 Damme^{5,6}, Lieven Clarisse⁴, Beatriz Herrera^{2,7}, Michel Grutter⁷, Pierre-Francois Coheur⁴, Kimberly
6 Strong², and Cathy Clerbaux^{1,5}.

7 ¹LATMOS/IPSL, Sorbonne Université, UVSQ, CNRS, 75252 Paris Cedex 05, France;

8 ²Department of Physics, University of Toronto, Toronto, ON M5S 1A7, Canada;

9 ³Department of Civil and Mineral Engineering, University of Toronto, Toronto ON M5S 1A4, Canada;

10 ⁴Department of Environmental Sciences, University of California, Riverside, CA 92521, USA;

11 ⁵Université libre de Bruxelles (ULB), Spectroscopy, Quantum Chemistry and Atmospheric Remote Sensing (SQUARES), Brussels 1050,
12 Belgium;

13 ⁶BIRA-IASB - Belgian Institute for Space Aeronomy, Brussels 1180, Belgium;

14 ⁷Instituto de Ciencias de la Atmósfera y Cambio Climático, Universidad Nacional Autónoma de México, Mexico City, 04510, Mexico;

15 *Correspondence:* Camille Viatte (camille.viatte@latmos.ipsl.fr)



16 **Abstract**

17 Megacities can experience high levels of fine particulate matter (PM_{2.5}) pollution linked to ammonia
18 (NH₃) mainly emitted from agricultural activities. Here, we investigate such pollution in the cities of
19 Paris, Mexico and Toronto, each of which have distinct emission sources, agricultural regulations, and
20 topography. Ten years of measurements from the Infrared Atmospheric Sounding Interferometer
21 (IASI) are used to assess the spatio-temporal NH₃ variability over and around the three cities.

22 In Europe and North America, we determine that temperature is associated with the increase in NH₃
23 atmospheric concentrations with coefficient of determination (r^2) of 0.8 over agricultural areas. The
24 variety of the NH₃ sources (industry and agricultural) and the weaker temperature seasonal cycle in
25 southern North America induce a lower correlation factor ($r^2 = 0.5$). The three regions are subject to
26 long range transport of NH₃, as shown using HYSPLIT cluster back-trajectories. The highest NH₃
27 concentrations measured at the city scales are associated with air masses coming from the
28 surrounding and north-northeast regions of Paris, the south-southwest areas of Toronto, and the
29 southeast/southwest zones of Mexico City.

30 Using NH₃ and PM_{2.5} measurements derived from IASI and surface observations from 2008 to 2017,
31 annually frequent pollution events are identified in the 3 cities. Wind roses reveal statistical patterns
32 during these pollution events with dominant northeast-southwest directions in Paris and Mexico
33 cities, and the transboundary transport of pollutants from the United-States in Toronto. To check
34 how well chemistry transport models perform during pollution events, we evaluate simulations made
35 using the GEOS-Chem model for March 2011. In these simulations we find that NH₃ concentrations
36 are overall underestimated, though day-to-day variability is well represented. PM_{2.5} is generally
37 underestimated over Paris and Mexico, but overestimated over Toronto.



38 1. Introduction

39 Paris, Toronto, and Mexico City are cities with over 2 million inhabitants. When their larger
40 metropolitan regions are included, their populations are 10.5 million for Paris (the most populous
41 area in the European Union), 6.5 million for Toronto (the fourth most populous city in North
42 America) and 9.2 million for Mexico City (most populous city in North America). These cities typically
43 experience strong particulate matter (PM) pollution episodes. Exposure to such particles is harmful
44 to humans and can lead to cardiovascular and respiratory diseases [Murray et al., 2020].

45 A large proportion of the particles' composition is ammonium sulfate and nitrate, which are formed
46 from ammonia (NH₃) [Behera et al., 2013] released in the atmosphere from e.g., fertilizer spreading
47 practices and both transported to cities, reducing the quality of urban air [Pope et al., 2009]. The
48 agricultural sector represents 94%, 90%, and 94% of total NH₃ emissions in France [CITEPA, 2018],
49 Canada [ECCC, 2017] and Mexico [INECC and SEMARNAT, 2018], respectively. NH₃ is the most poorly
50 understood precursor of PM_{2.5} (PM with a diameter less than 2.5 μm), primarily because
51 measurements are difficult [von Bobrutzki et al., 2010], sparse, and due to low ambient NH₃
52 concentrations and episodic emissions. Worldwide, only five countries have included NH₃
53 concentrations routine measurements in their air quality monitoring networks [Nair and Yu, 2020].

54 NH₃ emissions are associated with very high uncertainties in all inventories (186% to 294%
55 uncertainties in EDGAR [McDuffie et al., 2020; Van Damme et al., 2018]) due to uncertainties in the
56 reporting of agricultural statistics and emission factors that depend on individual agricultural
57 practices, biological processes, and environmental conditions [Paulot et al., 2014], as well as political
58 disturbances and land-use change [Abeed et al., 2021]. The evaporation of NH₃ in the atmosphere, as
59 well as its transformation into particulate matter, is highly dependent on the thermodynamic
60 conditions of the atmosphere [Sutton et al., 2013]. All these parameters account for the complexity
61 of reproducing NH₃ concentrations in atmospheric models, predicting the associated PM_{2.5} pollution,
62 and, ultimately, implementing relevant regulations to reduce its emissions.

63 Given the crucial role that NH₃ plays in environmental and public health problems, reducing its
64 emissions will therefore be a major challenge. However, NH₃ concentrations are increasing in all of
65 three regions, with a country wide increase of $24 \pm 11\%$, $16.4 \pm 8.6\%$, and $8.4 \pm 5.2\%$ between 2008
66 and 2018 in France, Canada, and Mexico, respectively [Van Damme et al., 2021].

67 In Paris, PM_{2.5} are composed with organic matter (38–47 %), nitrate (17–22 %), non-sea-salt sulfate
68 (13–16 %), ammonium (10–12 %), and to a minor extend with elemental carbon, mineral dust (2–5
69 %) and sea salt [Bressi et al., 2013]. In springtime, it has been shown that NH₃ plays a significant role
70 in PM_{2.5} pollution episodes [Viatte et al., 2021] but long-term observations are needed to properly
71 evaluate the impact of NH₃ to PM_{2.5} formation.

72 In Toronto, secondary nitrate formed with nitric acids (NO_x) and NH₃ account for 36% of the PM_{2.5}
73 sources [Lee et al., 2003] and ammonium nitrate and sulfate accounted for 20-30% of annual PM_{2.5}
74 mass over the 14-year period between 2006 and 2014 [Jeong et al., 2020]. There is a need for a
75 higher number of surface observations to evaluate the NH₃-PM_{2.5} relationship and its evolution over
76 time [Larios et al., 2018].

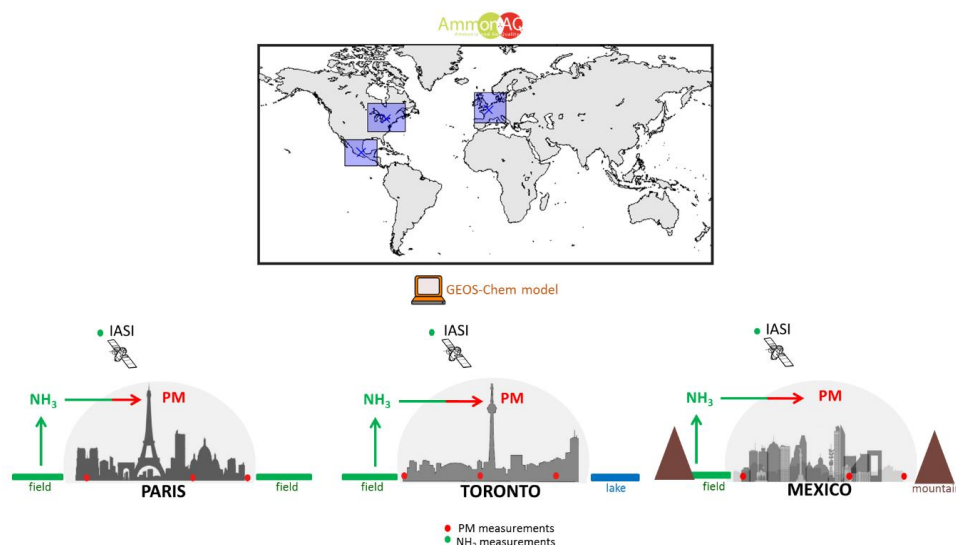
77 In Mexico, PM_{2.5} concentrations often exceed the standard of 65 μg/m³ [Moya and Huey, 2007;
78 INECC and SEMARNAT, 2018]. Secondary inorganic aerosols account for 30% of the chemical
79 composition of PM_{2.5}, which are dominated by ammonium sulfate with an average of 14% [Vega et
80 al., 2010]. A better understanding of the particulate pollutants processes in Mexico is still needed
81 [Ojeda-Castillo et al., 2019].



82 To assess the role of NH_3 in the formation of particulate matter, the AmmonAQ (Ammonia air
83 quality) project was designed to quantify NH_3 spatio-temporal variabilities in regional domains
84 around these three cities. The main objective of this project is to determine the impact of intensive
85 agricultural practices on NH_3 and urban air quality, with a focus on Paris, Toronto and Mexico as
86 benchmark case studies. A schematic representation of the AmmonAQ project and the domains of
87 study are shown in Figure 1. The so-called “Europe”, “North America”, and “southern North America”
88 domains represent the extended area with NH_3 sources that can impact on the Paris, Toronto, and
89 Mexico cities air composition. The three cities are investigated with the use of different datasets:
90 satellite measurements and model simulation data, and surface measurements when available (see
91 section 2).

92 These cities have been chosen as the focus of this study because of the availability of NH_3 and $\text{PM}_{2.5}$
93 measurements. These three cities differ in terms of:

- 94 1. The regulation of NH_3 emissions: French policies aim to reduce NH_3 emissions by 13% in 2030
95 relative to 2005 [CEIP, 2016] following EU ratification of the Gothenburg Protocol in 2017,
96 whereas in Canada and Mexico there are no federal regulations for NH_3 emissions yet
97 [Bittman et al., 2017];
- 98 2. Agricultural practices affecting NH_3 emissions differ in each region as farmers depend on
99 meteorological conditions for fertilizer use;
- 100 3. Meteorological/climate conditions are very different in each of the regions: drier winter and
101 wetter summer in Toronto compared to Paris, and weak winds and strong temperature
102 inversions in Mexico-city. This influences the NH_3 lifetime and chemistry leading to the
103 formation of $\text{PM}_{2.5}$;
- 104 4. Topography: Toronto is adjacent to Lake Ontario, Paris is inland, and Mexico-city is a basin
105 surrounded by mountains. This will impact the trajectories of air masses.



106

107 Figure 1: schematic representation of the AmmonAQ project. Upper panel: the three study regions investigated
108 (in blue rectangles). Lower panel: presentation of each city and regional domain and different datasets used.

109



110 2. Methodology

111 2.1. NH₃ observations derived from IASI

112 The Infrared Atmospheric Sounding Interferometer (IASI) was launched onboard the Metop-A/B/C
113 satellites in 2006, 2012, and 2018, respectively [Clerbaux et al., 2009]. IASI provides twice daily total
114 column measurements of NH₃ globally at 9:30 and 21:30 local solar time. With its polar orbit and a
115 swath of 2400 km, IASI pixel size is 12 km in diameter at nadir. In this work, we use version 3 of the
116 ANNI-NH₃ product [Van Damme et al., 2021; Guo et al., 2021] from IASI Metop-A/B morning
117 overpasses over the period 2008 to 2017.

118 2.2. PM_{2.5} dataset derived from surface network measurements

119 To study local scale PM_{2.5} pollution events in the Paris, Toronto, and Mexico cities, PM_{2.5} observations
120 of surface concentrations from 2008 to 2017 are used.

121 For Paris, we use hourly observations of PM_{2.5} concentrations derived from fourteen stations of the
122 Airparif network (<https://data-airparif-asso.opendata.arcgis.com/>). For Toronto, we analyze hourly
123 PM_{2.5} observations derived from eleven stations supported by the Ministry of the Environment,
124 Conservation and Parks of Ontario (<http://www.airqualityontario.com/>). For Mexico, PM_{2.5}
125 concentrations are derived from 27 stations of the Red Automática de Monitoreo Atmosférico
126 (RAMA, <http://www.aire.cdmx.gob.mx/default.php?opc=%27aKBh%27>) network.

127 All these stations are located in a 50-km radius-circle around the city centers of Paris, Toronto, and
128 Mexico City.

129 2.3. NH₃ and PM_{2.5} from the GEOS-Chem model

130 We generate model outputs for March of 2011 using version 12.7.2 of the GEOS-Chem chemical
131 transport model [Bey et al., 2001] driven by the MERRA-2 reanalysis product, including nested
132 domains over Europe and North America at a 0.5° × 0.625° horizontal resolution from which we
133 extract modeled surface values for each city. Boundary conditions for these two nested domains are
134 created using a global simulation for the same months at 2° × 2.5° resolution. Output for the
135 analyzed month of March includes monthly means, as well as hourly means for selected diagnostics,
136 and is preceded by two months of discarded model spinup time for the global simulation, and one
137 month for each nested run. Anthropogenic emissions are taken primarily from the global Community
138 Emissions Data System (CEDS) inventory [Hoesly et al., 2018], with regional emissions from the 2011
139 National Emissions Inventory produced by the US EPA (NEI2011) used to override global values over
140 the United States. Biogenic non-agricultural ammonia, as well as ocean ammonia sources, are taken
141 from the Global Emission Inventories Activities database (GEIA, [Bouwman et al., 1997]). Open fire
142 emissions are generated using the GFED 4.1s inventory [Randerson et al., 2017]. Sulfate-nitrate-
143 ammonium aerosol processes are calculated using version 2.2 of the ISORROPIA thermodynamic
144 module [Fountoukis and Nenes, 2007]. Black carbon is handled as described in Wang et al. (2014),
145 while secondary organic aerosol is produced using the simplified irreversible scheme described in Pai
146 et al., (2020).

147 2.4. Back-trajectories analysis from the HYSPLIT model

148 To determine the effect of long-range transport affecting the local air quality of the three cities, we
149 use the Hybrid Single-Particle Lagrangian Integrated Trajectory model (HYSPLIT, [Stein et al., 2015]).
150 One note that unlike the GEOS-Chem model, HYSPLIT does not include atmospheric chemistry. For
151 the runs, meteorological data are from the National Centers for Environmental Prediction (NCEP) /



152 National Center for Atmospheric Research (NCAR) reanalysis at 2.5-degree global latitude-longitude
 153 projection. First, we run daily 24-hours back-trajectories ending in the city-centers at the overpass
 154 time of the IASI instrument covering the period 2008 to 2017. Then, for each day we calculate the
 155 mean of NH_3 total columns derived from IASI observations in a 50-km radius circle around the cities
 156 associated with each back-trajectory. Finally, every back-trajectory are combined in clusters and
 157 associated with the corresponding local-scale IASI NH_3 concentrations.

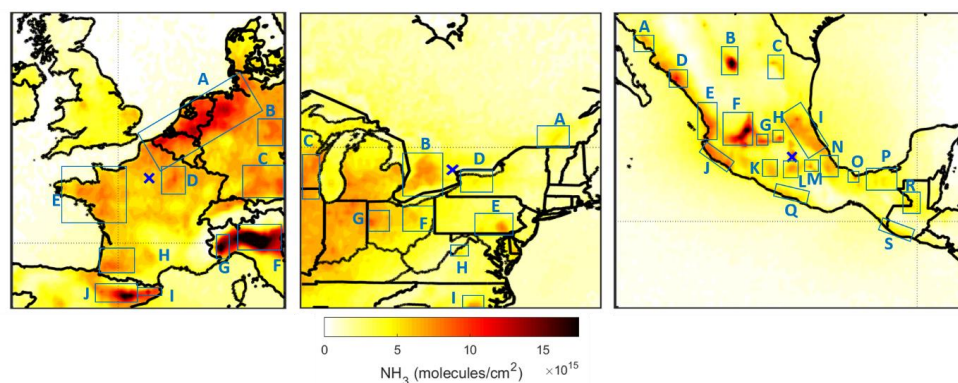
158 2.5. ERA-5 meteorological data

159 The meteorological variables used in this study are extracted from the hourly ECMWF's reanalysis
 160 (ERA5, [Hersbach et al., 2020]). ERA5 data are at $0.25^\circ \times 0.25^\circ$ resolution (native horizontal resolution
 161 of ERA5 is $\sim 31\text{km}$) and are interpolated in time and space to the IASI observation. The meteorological
 162 parameters considered here are the skin temperature (T_{skin} , which is the physical temperature of
 163 the Earth's surface), total precipitation (in meter of water equivalent - accumulated liquid and frozen
 164 water, comprising rain and snow -) and relative humidity up to 2 meters above the surface calculated
 165 from dew and air temperature at 2m from ERA5.

166 3. Results

167 3.1. NH_3 source regions identification and spatio-temporal variability over the Europe, 168 North America, and southern North America domains

169 Using 10-years of IASI observations, the main source regions of NH_3 in the 3 domains of study are
 170 identified (Figure 2) and listed in Table 1. We identify 10, 9, and 19 NH_3 source regions over the
 171 Europe, North America, and southern North America regions, respectively. All of the sources over the
 172 Europe, North America domains are mostly related to agricultural practices (farming and spreading
 173 practices). This is in agreement with previous calculation of worldwide nitrogen inputs from fertilizer
 174 and manure [Potter et al., 2010]. Around southern North America, three sources are related to
 175 fertilizer or soda ash industries (listed with C, G, O in Figure 2 and Table 1, [Van Damme et al., 2018]),
 176 the rest is agricultural.



177
 178 Figure 2: Source region identification of NH_3 derived from 10 years average of IASI total columns
 179 (molecules/cm^2) from 2008 to 2017. The blue crosses indicate Paris, Toronto, and Mexico cities locations.

180 Spatio-temporal variabilities of NH_3 in the atmosphere in the three regions (Figure 2) are not
 181 expected to be similar: NH_3 emissions from industries in the region of southern North America are
 182 released all year long, whereas NH_3 emissions from agricultural practices (i.e. major over Europe and
 183 North America), depend on various surface and meteorological conditions. In order to investigate



184 this, NH₃ concentrations using 10-years of IASI observations are assessed against atmospheric
 185 temperature and precipitation derived from the ERA5 reanalysis over the three domains in Figure 3.
 186 It shows the seasonal evolution of NH₃ from IASI over the three regions (left panel), along with the
 187 seasonal evolution of temperature and precipitation (right panel).

188 Table 1: List of NH₃ source regions identified using 10-years average of IASI total columns (molecules/cm²) over
 189 the Europe, North America, and southern North America regions.

Europe [41°-59°N ; -11.25°- 16.25°E]		North America [35°-53°N ; 93.75°-63.75°W]		Southern North America [9°-29°N ; 113.75°-86.25°W]	
A	The North-European plain ^{1,2}	A	Granby	A	Obregon (Mexico) ¹
B	Saxe Anhalt plain (Germany)	B	Elmira-Kitchener-Guelph	B	Torreon (Mexico) ^{1,2}
C	Munich - Mangfall (Germany)	C	Brillion area	C	Garcia (Mexico)** ¹
D	Champagne-Ardennes (France)	D	New-York state	D	Culiacancito (Mexico) ^{1,2}
E	Bretany-Pays de la Loire (France) ²	E	Lancaster county	E	Nayarit (Mexico)
F	Pô Valley (Italy) ^{1,2}	F	Wayne county	F	Jalostotitlan-San Juan de Los Lagos (Mexico) ^{1,2}
G	Valley of piedmont (Italy) ^{1,2}	G	Celina-Coldwater ¹	G	Salamanca – Villagran (Mexico)* ¹
H	Landes area (France)	H	Shenandoah Valley- Bridgewater ¹	H	Ezequiel Montes (Mexico) ^{1,2}
I	Vic - Manlleu (Spain) ^{1,2}	I	Lenoir County	I	Tampaon, Loma Alta (Mexico) ¹
J	Ebro river basin (Spain) ^{1,2}			J	Tecoman (Mexico)
				K	Coyuca de Catalan (Mexico)
				L	Morelos (Mexico)
				M	Tochtepec-Tehuacan (Mexico) ¹
				N	South of Veracruz (Mexico)
				O	Cosolaecaque (Mexico)* ¹
				P	Tabasco (Mexico)
				Q	Guerrero (Mexico)
				R	Chisec (Guatemala)
				S	Texcuaco (Guatemala)

*Fertilizer industry ** Soda ash industry

¹ Van Damme et al., 2018; Clarisse et al., 2019

² Dammers et al., 2019

190

191 For Europe and North America, NH₃ total columns are the highest in spring and summer. In fact, NH₃
 192 concentrations over Europe exhibit two seasonal maxima in March/April and July/August
 193 (supplementary material, Figure S1) and in North America the maxima are in May and September
 194 (Figure S2). This is consistent with agricultural practices (i.e. fertilizer application) and higher air
 195 temperature favoring NH₃ volatilization in the atmosphere.

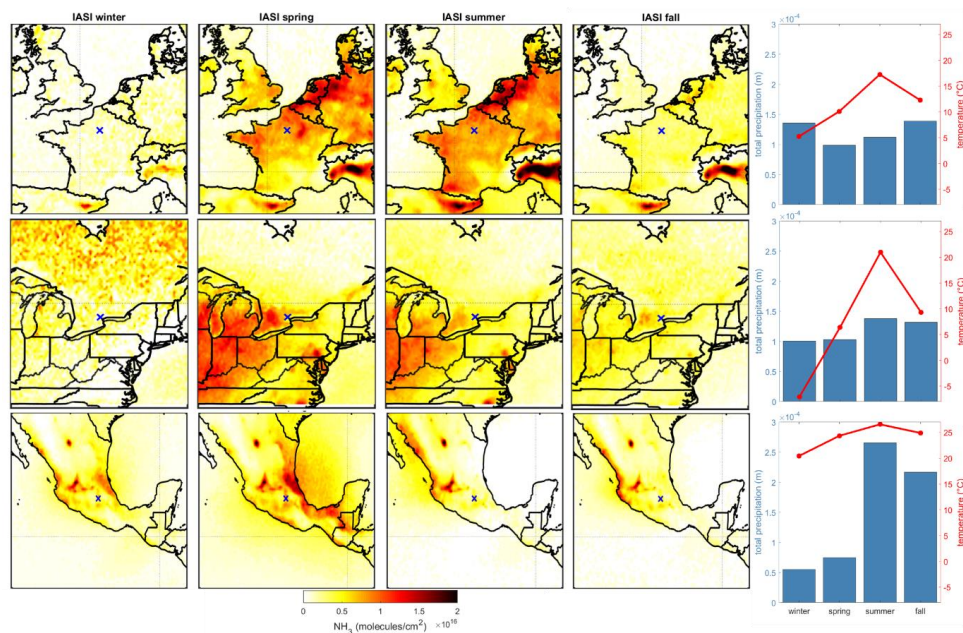
196 The right panel of Figure 3 shows how temperature (red lines) and precipitation (blue bars)
 197 seasonally evolve over the three regions. In winter, atmospheric temperatures are below 5 °C in
 198 Europe and North America, and IASI observations reveal almost no NH₃ hot spots (left panel, Figure
 199 3). This can be due to the lack of NH₃ abundance, lower volatilization in this temperature range, no
 200 agricultural emissions in winter and/or the reduced sensitivity of the IASI NH₃ retrievals in winter
 201 [Van Damme et al., 2017].

202 In southern North America, NH₃ seasonal variations are less pronounced than in the other two
 203 regions. Figure 3 shows that the NH₃ concentrations over several sources, such as Torreon and San
 204 Juan de Los Lagos (boxes B and F in Figure 2 right panel) are high during all seasons, which could be
 205 associated with the weak seasonal cycle of temperature in this region close to the equator.

206 In spring, seasonal precipitations are the lowest for the three regions. This is reflected in high NH₃
 207 concentrations on the left panel. Over Europe and North America, this can be related to agricultural
 208 spreading practices period and higher atmospheric temperature favoring NH₃ volatilization. In
 209 southern North America, NH₃ concentrations observed by IASI are the highest in spring when
 210 atmospheric temperatures are high and precipitations rates are low. In addition, biomass burning,



211 that are often encountered during this period could explain higher atmospheric NH₃ concentrations
 212 in spring. NH₃ reach maximum values in April/May (Figure S3) just before the start of the rain season,
 213 potentially reducing observed NH₃ concentrations due to the wet deposition of atmospheric gaseous
 214 ammonia [Asman et al., 1998].



215

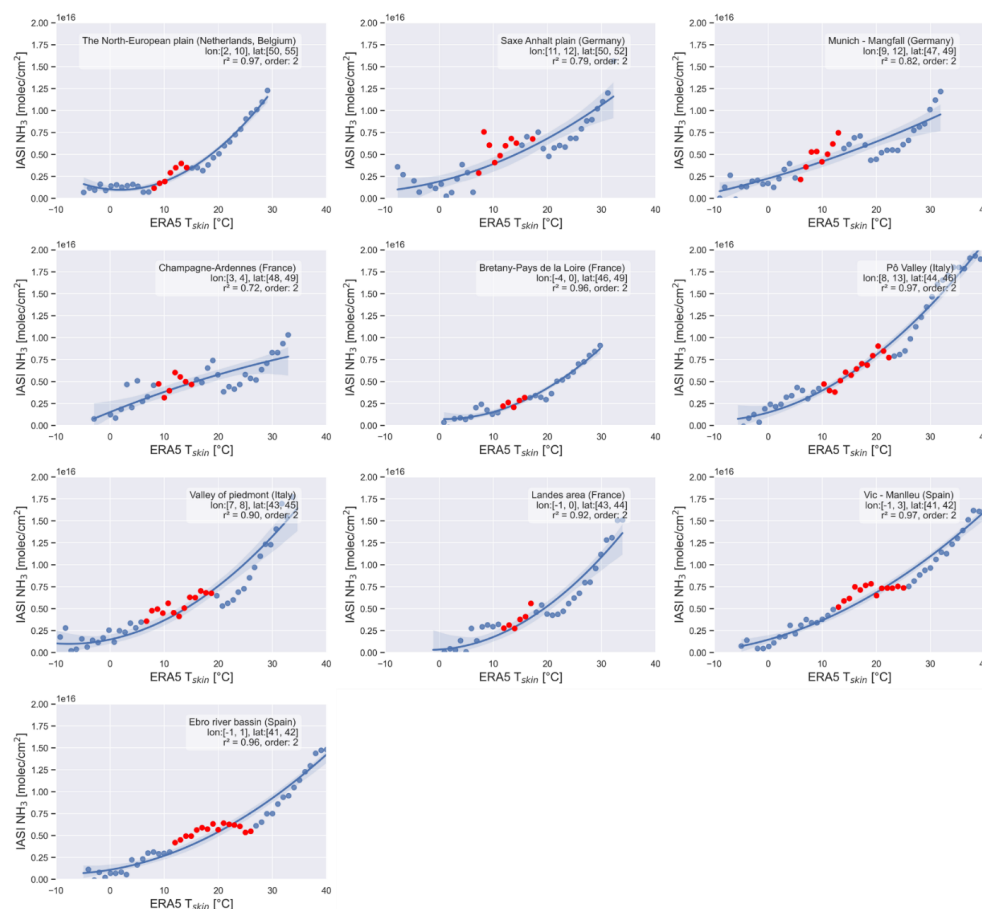
216 Figure 3: Seasonal maps of NH₃ total columns (molecules/cm²) derived from 10 years (2008-2017) of IASI
 217 observations, along with seasonal means of atmospheric temperature (red line) and precipitation (blue bar
 218 chart) over the Europe (upper panels), North America (middle panels), and southern North America (lower
 219 panels) regions.

220 Since in Europe and North America NH₃ sources are mostly agriculture-related (with a mild
 221 contribution from industries), the temperature/NH₃ relationship is expected to be relatively easy to
 222 interpret: when the land surface temperature increases, volatilization of ammonia from the
 223 fertilized/manured soil is favored, and atmospheric ammonia increases. The corresponding
 224 determination factors r^2 for this relationship in Europe and North America are 0.85 and 0.80
 225 respectively (polynomial fit of second order). This is not the case in southern North America, in which
 226 some of the ammonia sources are also industrial and they contribute greatly to the atmospheric NH₃,
 227 the concentrations of ammonia are therefore not directly temperature dependent, as we can see on
 228 the right upper panel in Figure S4 ($r^2 = 0.46$). There is nonetheless a relationship in southern North
 229 America that is due to the fact that we have constant high ammonia sources and temperatures
 230 (Figure 3). In fact, the relationships between NH₃ and temperature on one hand, and
 231 precipitation/relative humidity on the other hand, are not linear; this has been equally shown in a
 232 previous study [Sutton et al., 2013].

233 To further investigate the temperature/NH₃ relationship, we show in Figure 4 the evolution of NH₃
 234 with respect to land surface temperature over different sub-regions of the Europe domain (listed in
 235 Table 1). Similar Figures for the North America and southern North America domains are shown in
 236 the supplement information (Figure S5 and S6). We observe a peak of NH₃ followed by a local



237 maximum plateau between 10 and 25°C approximately in all of the regions of the Europe domain
 238 (Figure 4). In fact, the NH₃ detected in this range of temperature can indicate the fertilizer application
 239 period, since most of them (up to 80%) were detected during the spring and fall seasons. For
 240 instance, over the Po valley (region F in Table 1, Figure 4), 36% of the NH₃ detected in the bins 10 –
 241 25°C correspond to the spring season, whereas 35% correspond to the fall season (not shown here).
 242 In Celina-Coldwater (region G in Table 1), 82% of the NH₃ detected between 10 and 25°C correspond
 243 to the spring and the fall seasons, the percentage is split equally (Figure S5).



244
 245 Figure 4: Yearly IASI NH₃ total columns (molecules/cm²) averaged per bins of ERA5 skin temperatures (°C), with
 246 an interval of 1°C between each consecutive bin. The red circles denote the growing seasons, at least 60% of
 247 the NH₃ is detected during March-May and Sept-Nov periods. See Figure 2 and Table 1 for the localization of
 248 the sub-regions around Europe.

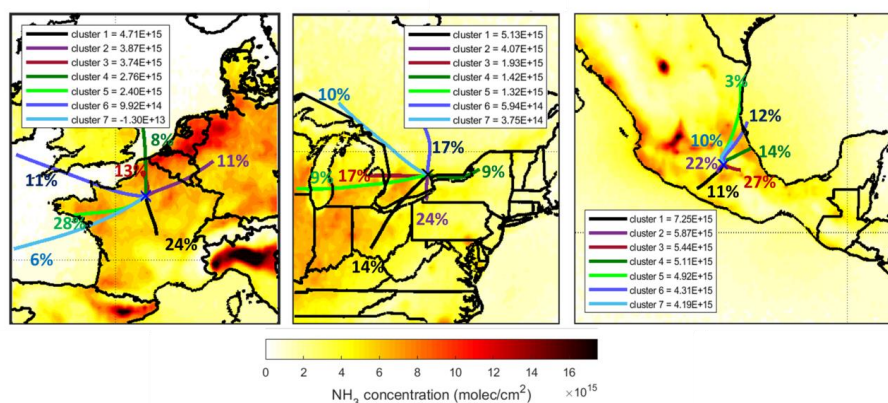
249 We choose to show the sub regions in the vicinity of the Europe domain, since they are mostly
 250 agricultural sources. The “bumps” corresponding to the fertilizer application are very clear in all of
 251 the sub-regions. This bump was detected to a lower extent for agricultural regions affecting North
 252 America (supplementary material Figure S5). Over the agricultural regions in the southern North
 253 America domain, the bumps are clear in the regions A to D (Figure S6, a). When the seasonal
 254 temperatures do not fluctuate during the fertilizer application, any increase in atmospheric NH₃ is



255 due to the sudden addition of nitrogen fertilizers in the soil. In southern North America, the regions E
 256 to M show that the highest NH_3 concentrations were observed as the temperature increased during
 257 the growing seasons (Figure S6). A possible explanation to the resemblance among the regions A to D
 258 is that they share similar climate properties (Steppe and Desert) unlike the rest of the sub-regions in
 259 the same domain (tropical/subtropical). Since the temperatures in the Europe and southern North
 260 America domains are higher (Figure 3, right panels) in spring and fall seasons (fertilizer application
 261 period) than those in North America, this bump is clearer in the latter. The bumps seen for the
 262 Europe regional domain are clearer than those of southern North America, possibly related to the
 263 fact that in autumn in Europe precipitation is lower than those in southern North America, leading to
 264 lower NH_3 loss through wet deposition.

265 3.2. NH_3 budget over the cities of Paris, Toronto, and Mexico

266 Temperature, relative humidity, and precipitation are not the only factors affecting the NH_3
 267 concentrations. More locally, and to analyze the impact of long-range transport on NH_3
 268 concentrations measured over the cities (and not domains) of Paris, Toronto, and Mexico, HYSPLIT
 269 back-trajectories have been used. For each day of IASI NH_3 observations made in a 50-km radius
 270 circle from the city-center, a 24-hours back-trajectory has been performed from 2008 to 2017. There
 271 are between 3643 and 4008 back-trajectories for Paris, Toronto, and Mexico cities. Then, a seven-
 272 cluster analysis has been applied to these datasets and NH_3 mean concentrations measured inside
 273 the cities by IASI have been allocated to the different mean cluster trajectories. The result is shown in
 274 Figure 5.



275

276 Figure 5: Seven cluster-mean backward trajectories over the Europe, North America, and southern North
 277 America regions for the whole time period between 2008 and 2017. Back-trajectories are color-coded in
 278 function of the corresponding NH_3 concentrations measured inside the cities. The numbers indicate the
 279 percentage of trajectories allocated to a cluster.

280 For Paris, 1/4 of all back-trajectories (875) that are associated with the most NH_3 concentrations, i.e.
 281 $4.71 \cdot 10^{15}$ molecules/cm² on average, are coming from the surrounding south regions (black line,
 282 Figure 5). Clusters 2 and 3 are also associated with high NH_3 concentrations and are coming from the
 283 north-northeast. This is consistent with previous analyses using HYSPLIT [Viatte et al., 2020] and
 284 FLEXPART models [Viatte et al., 2021]. As expected, the back-trajectories coming from the ocean are
 285 related with almost no NH_3 concentrations (light and dark blue lines, left panel).



286 Over Toronto, the highest NH_3 concentrations (24% and 14%) measured in the city are allocated to
 287 long-range transport located south-southwest (black and purple lines, middle panel) coming from the
 288 United-States where most of the feedlots are. 9 to 17% of NH_3 concentrations are coming from the
 289 west and the east of Toronto (cluster 3, 4, and 5) where sources emissions have increased in the last
 290 decade [Yao and Zhang, 2019]. The 2 back-trajectory clusters that are related to low NH_3
 291 concentrations are coming from the north (light and dark blue lines) where no NH_3 sources have
 292 been identified.

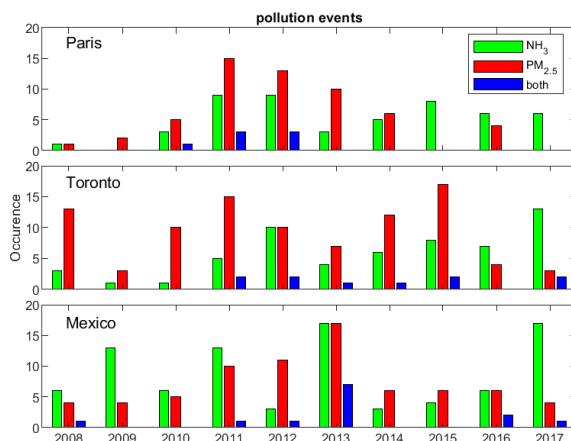
293 In the southern North America domain, back-trajectories are coming from relatively close regions
 294 since orographic conditions around Mexico-city limit long-range transport. In this city, the highest
 295 NH_3 concentrations are associated with air masses coming from the southwest (11%, black line, 22%,
 296 purple line, right panel) and southeast (27%, red line). Air parcels coming from the north are
 297 associated with relatively low NH_3 concentrations measured in Mexico City.

298 3.3. Pollution events over Paris, Toronto, and Mexico cities from 2008 to 2017

299 After assessing the NH_3 distribution under average climate conditions, we focus now on pollution
 300 events occurring at the 3 cities. These are identified by applying the Fourier series of order 3
 301 [Yamanouchi et al., 2021; Herrera et al., 2022] on the surface $\text{PM}_{2.5}$ and satellite NH_3 observations at
 302 cities scale (i.e. 50-km radius circle from city-centers). The Fourier fit accounts for the “natural”
 303 variability (seasonality) in the time-series, and helps identify pollution events that are above this
 304 natural variability. It is a robust method commonly used to quantify trends and identify
 305 enhancements in long-term timeseries [Zellweger et al., 2009]. Pollution events occurrence per year
 306 and per city are shown in Figure 6.

307 The figure shows that NH_3 pollution episodes are found to be annually frequent at the 3 cities. In
 308 Toronto and Mexico cities, $\text{PM}_{2.5}$ pollution events are encountered annually (with higher number in
 309 Mexico) whereas no events are detected in 2009, 2015, and 2017 in Paris.

310 Numbers of identified days of $\text{PM}_{2.5}$ pollution events are 88, 58, and 50 in Mexico City, Toronto, and
 311 Paris, respectively. For NH_3 pollution events, they occur more in Toronto than in Mexico City and
 312 Paris, with number of days of 94, 73, and 56, respectively. Common days of high NH_3 and $\text{PM}_{2.5}$
 313 concentrations are found in all 3 cities, especially in spring (not shown here), coinciding with the high
 314 seasonal NH_3 concentrations shown in Figure 3.





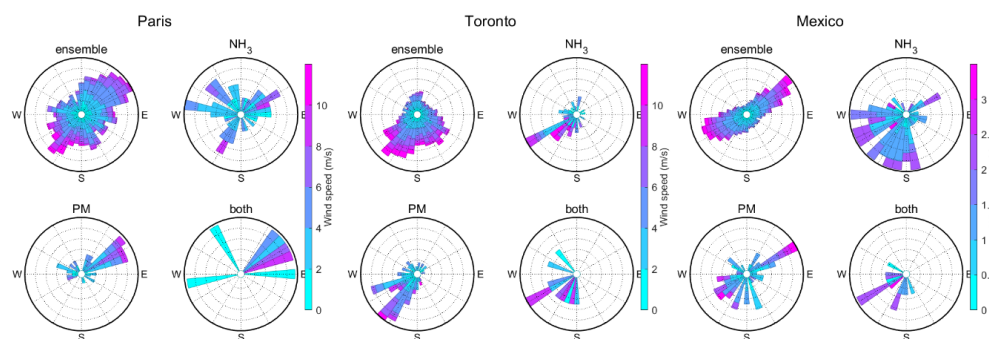
316 Figure 6: Annual occurrence of pollution events of NH₃ (green bars), PM_{2.5} (red bars), and NH₃ and PM_{2.5}
 317 simultaneous (blue bars) detected from 2008 to 2017 in Paris (upper panel), Toronto (middle panel), and
 318 Mexico (lower panel) cities.

319 To further investigate the impact of transport on pollution events occurring at the 3 cities, we have
 320 analyzed the wind fields patterns for different cases: i) for the whole dataset (i.e. ensemble 2008-
 321 2017), ii) for days of NH₃ and PM_{2.5} pollution events occurred separately, and iii) for days when both
 322 high concentrations are monitored. Figure 7 shows wind roses computed for the ensemble and these
 323 different types of pollution events (i.e. PM_{2.5}, NH₃ and both occurring during the same day). In
 324 general, wind speed is lower at Mexico City (max 3 m.s⁻¹) compared to Toronto and Paris (up to 10
 325 m.s⁻¹) because of the mountainous topography that blocks and slows air masses exchange in Mexico.

326 In Paris, the ensemble wind-roses show a dominant northeast-southwest pattern. NH₃ pollution
 327 events are associated with wind coming from various directions at all wind speeds which was
 328 suggested by the HYSPLIT cluster analysis (Figure 5), whereas PM_{2.5} events are present mainly under
 329 high northeast wind. When both NH₃ and PM_{2.5} high concentrations are observed in Paris, the wind
 330 field can have two patterns: low wind speed coming from all direction (except from the south) or
 331 high wind speed coming from the northeast. This confirms the importance of transport of NH₃ and
 332 PM_{2.5} from the northeast and could suggest the inter-conversion of PM_{2.5} to NH₃ at low wind speed.

333 In Toronto, the ensemble show that dominant wind pattern is coming from the south. For all the
 334 pollution events (NH₃, PM_{2.5}, and both) the wind is coming from the southwest, confirming the long-
 335 range transport of pollutants from the United-States.

336 In Mexico City, the dominant pattern (ensemble) is southwest-northeast wind fields. For days of NH₃
 337 pollution events, wind is mainly coming from the south-southwest, and for PM_{2.5}, wind come from all
 338 direction with an important northeast wind pattern. Days of both pollution events are associated
 339 with wind coming from the west-southwest only.



340

341 Figure 7: Wind roses corresponding to the ensemble of all observations, the NH₃, PM_{2.5}, and both NH₃ and
 342 PM_{2.5} simultaneous pollution events derived from 2008 to 2017 over Paris (left panels), Toronto (middle
 343 panels), and Mexico (right panels) cities.

344 3.4. Case study: NH₃ and PM_{2.5} concentrations comparison with the GEOS-Chem model in 345 March 2011

346 The occurrence of pollution events varies from year to year (Figure 6). However, in 2011, all 3 cities
 347 experienced PM_{2.5} and NH₃ separate and combined pollution events. For this reason, GEOS-Chem



348 model simulations were performed in March 2011 to interpret the events and evaluate the model
349 performance.

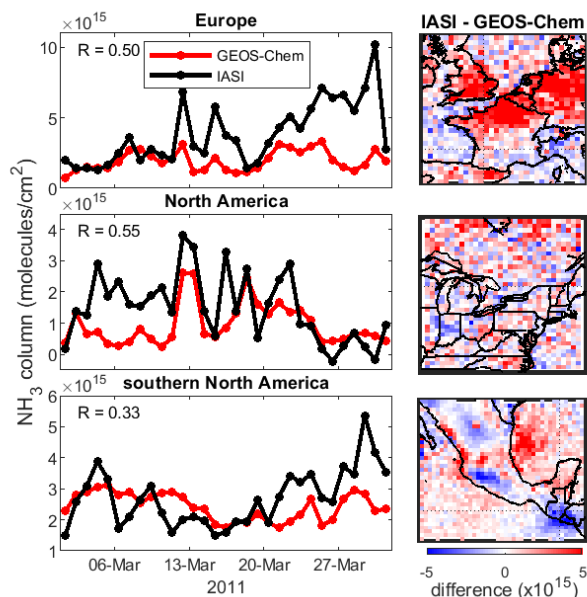
350 Spatial and temporal coincidence criteria have been applied to GEOS-Chem outputs to compare with
351 IASI morning observations. We have selected collocated model outputs between 8.30 and 11.30 AM
352 coincident with IASI overpasses. Averages of numbers of IASI observations are 1324, 1138, and 3000
353 over the Europe, North America, and southern North America domains of study during March 2011.

354 Figure 8 shows the one-month comparison between the two datasets. Over the regional domains,
355 the coefficient of correlation between daily model NH_3 concentrations and IASI NH_3 observations are
356 $R = 0.50$, $R = 0.55$, and $R = 0.33$, over Europe, North America, and southern North America,
357 respectively, with related p -values < 0.01 . NH_3 columns derived from the GEOS-Chem model are
358 overall underestimated with Mean Relative Difference (MRD = (observations - model) / model) of
359 104%, 109%, and 12% over Europe, North America, and southern North America, respectively.

360 Over Europe and North America, day-to-day variabilities are in agreement since IASI and GEOS-Chem
361 exhibit same enhancements (on March 12, 15, and 30 over Europe, and March 12, 13, and 18 over
362 North America). In southern North America, the underestimation of the GEOS-Chem NH_3 columns is
363 less pronounced (MRD is 12%) than in the other regions but the day-to-day variability is not well
364 represented in the model.

365 The GEOS-Chem model NH_3 total columns are lower than those from IASI in March 2011 over specific
366 locations in the southern North America and Europe domains (Figure 8, right panels). For the Europe
367 region, GEOS-Chem NH_3 columns are smaller than the IASI ones over the north of France, Belgium,
368 the Netherlands, north of Spain (in particular sources A, B, C, D, E, I, and J of Figure 2) and the United
369 Kingdom. For the southern North America domain, GEOS-Chem NH_3 columns are smaller than the
370 IASI ones over the west Mexican coast (sources A, D, E, J of Figure 2/Table 1), central (source F, G, H
371 of Figure 2) and southeast (sources O and P of Figure 2) of Mexico City and over the Pacific Ocean,
372 whereas they are higher in Guatemala (source S, R of Figure 2), and West of Mexico City.

373 Over the North America domain, spatial distribution of the differences between NH_3 columns derived
374 from GEOS-Chem and IASI are less pronounced than in the Europe and southern North America
375 domains. IASI NH_3 columns are smaller than GEOS-Chem outputs over the south of the United-States
376 and over the Lancaster County (sources E and I of Figure 2) and higher over Indiana in the United
377 States.

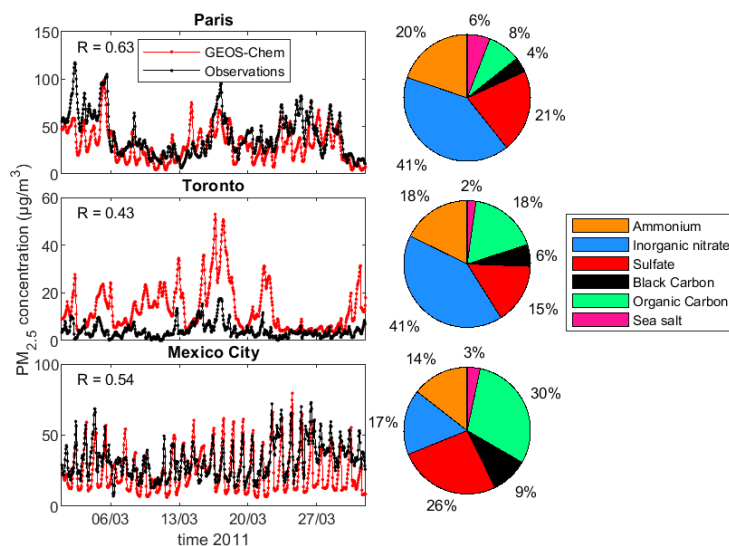


378

379 Figure 8: Left: time-series of daily NH_3 columns derived from IASI (black lines) and the GEOS-Chem model (red
 380 lines) over Europe (upper panel), North America (middle panel), and southern North America (lower panel).
 381 Right: maps of NH_3 columns (in molecules/ cm^2) differences between IASI and GEOS-Chem model for March
 382 2011.

383 At the city scales of Paris and Mexico City, the daily model NH_3 columns are in relatively good
 384 agreements with IASI observations within a 50-km radius circle from the city-centers (not shown
 385 here), since the coefficient of correlation are $R = 0.42$ and $R = 0.52$, respectively. Similar to the
 386 regional domains, GEOS-Chem NH_3 columns are relatively underestimated at the city scales of Paris
 387 and Mexico City, with a MRD of 14% and 72%. At the city scale of Toronto, the correlation between
 388 the NH_3 columns derived from the model and observed by IASI is poor, with a coefficient of
 389 correlation of $R = -0.32$, and an overestimation of the modelled NH_3 concentrations is found with a
 390 MRD of -81%.

391 Local comparison of $\text{PM}_{2.5}$ concentrations at the city scale (over Paris, Toronto, and Mexico) is shown
 392 in Figure 9, left panels. They show that $\text{PM}_{2.5}$ concentrations calculated by the model in March 2011
 393 are in relatively better agreement with the surface observations with $R = 0.63$, $R = 0.43$, and $R = 0.54$
 394 in Paris, Toronto and Mexico City. In Paris and Mexico City, $\text{PM}_{2.5}$ concentrations values derived from
 395 the observations are overall higher than the GOES-Chem concentrations with MRD values of 55% and
 396 65%, respectively, whereas GEOS-Chem $\text{PM}_{2.5}$ concentrations are higher than the observations in
 397 Toronto with MRD value of -59%.



398

399 Figure 9: left: Time-series of hourly PM_{2.5} (µg/m³) derived from surface observations (black lines) and the GEOS-
 400 Chem model (red lines) over Paris (upper panel), Toronto (middle panel), and Mexico (lower panel) cities for
 401 March 2011. Right: PM_{2.5} speciation (% in total mass) derived from the GEOS-Chem run for March 2011.

402 The right panels of Figure 9 show the chemical composition of the PM_{2.5} from GEOS-Chem. These
 403 inform us about the different pollution sources. Organic matter sources split equally between the
 404 primary emissions and the oxidation of volatile organic compounds [Day et al., 2015]. SNA (sum of
 405 sulfate, nitrate, and ammonium) sources originate in chemical transformation of gaseous precursors
 406 in the atmosphere, whereas black carbon comes from primary emissions of industrial and traffic
 407 combustion.

408 According to the GEOS-Chem model, SNA dominates the PM_{2.5} chemical composition mass in March
 409 2011 over the 3 cities, meaning that the dominant source of PM_{2.5} mass comes from the secondary
 410 oxidation path. This partition of SNA in March 2011 from the model is higher than what have been
 411 reported based on 1-year-measurements performed in 2013: 43%, 42%, and 33% of the PM_{2.5} mass
 412 composition in Paris, Toronto, and Mexico City, respectively [Cheng et al., 2016].

413 In Toronto, PM_{2.5} speciation is monitored by the National Air Pollution Surveillance Program (NAPS,
 414 [https://www.canada.ca/en/environment-climate-change/services/air-pollution/monitoring-
 415 networks-data/national-air-pollution-program.html](https://www.canada.ca/en/environment-climate-change/services/air-pollution/monitoring-networks-data/national-air-pollution-program.html)) network. Observations in March 2011 reveal
 416 that inorganic nitrate burden is overestimated by a factor 2 in the GEOS-Chem run (41% in the model
 417 compared to 20% in the observations), whereas sulfate and black carbon abundances are
 418 underestimated by a factor 2 (15 and 6% in the model compared to 27 and 12% in the observations).

419 In Mexico City, the organic matter represents the most abundant fraction of the aerosol, which is
 420 consistent with measurements made during several campaigns performed in the dry season of 2006
 421 during the Megacity Initiative: Local And Global Research Observations (MILAGRO, [Molina et al.,
 422 2010]) and Aerosoles en Ciudad Universitaria (ACU) in 2015 [Salcedo et al., 2018]. Daily cycles appear
 423 overexaggerated in the model with maxima well represented and minima greatly underestimated.



424 This could suggest model issues in term of atmospheric dynamics (removal/transport or planetary
425 boundary layer dynamics) due to coarseness of grid.

426 **4. Conclusion**

427 The AmmonAQ project aims to determine the impact of intensive agricultural practices on urban
428 pollution in the Paris, Toronto, and Mexico metropolitan areas. For this purpose, PM_{2.5} and NH₃
429 measurements from in situ instruments and satellite infrared spectrometers, and atmospheric model
430 simulations, have been combined.

431 Using 10-years of IASI observations, NH₃ sources regions have been identified. All of the sources are
432 from the agricultural sector (husbandry and fertilizer application) in the Europe and North America
433 domains, whereas, some of them are industrial in the southern North America region. Consequently,
434 the spatio-temporal variability of NH₃ is different, with stronger seasonal variabilities in Europe and
435 North America. A strong correlation is found between NH₃ total columns and surface temperature
436 (T_{skin}) for all regions, with higher correlation over agricultural regions, and when the temperature
437 seasonal cycle is pronounced. We find that the timing of the fertilizer application can be detected
438 through local maxima in the NH₃/T_{skin} relationship curve.

439 According to HYSPLIT cluster analysis, the highest NH₃ concentrations measured at the city scales are
440 associated with air masses coming from the surrounding regions and the north-northeast of Paris,
441 the south-southwest of Toronto, and the southeast/southwest of Mexico City. These will lead to the
442 exacerbation of the degradation of air quality in each of the 3 cities.

443 Pollution episodes are found to be annually frequent at the 3 cities, especially in springtime when
444 high NH₃ and PM_{2.5} are observed. In Paris and Mexico, winds are coming from the northeast-
445 southwest directions, whereas, in Toronto, the transboundary transport of pollutant from the
446 United-States is dominant during pollution events.

447 The evaluation of the GEOS-Chem outputs in March 2011 reveals that NH₃ concentrations are overall
448 underestimated by the model at the regional scale, with, however, a good representability of the
449 day-to-day variability in Europe and North America domains. NH₃ columns derived from IASI and the
450 GEOS-Chem model exhibit substantial spatial differences in the Europe and southern North America
451 areas. In term of PM_{2.5} concentrations at the city scales, we show that they are underestimated in
452 Paris and Mexico, but overestimated in Toronto.

453 The IASI thermal infrared remote sensors have proved to be valuable to monitor pollution events
454 over cities. The main limitations are associated with the low revisit time (at the beginning and at the
455 end of the day), the lack of sensitivity to the surface in particular in winter, and some areas are not
456 well covered during cloudy scenes. In the near future the next generation of instruments will have
457 improved capabilities to sound deeper in the atmosphere [Crevoisier et al., 2014]. The IRS-MTG
458 satellite instrument that should be launch in 2024 in geostationary orbit will offer the capacity to
459 enhance this research over Europe thanks to better temporal (measurements every 30-45 minutes)
460 and spatial (4 km x 4 km pixel) resolution.

461 **Data availability**

462
463 The near-real-time IASI NH₃ (ANNI NH₃-v3) data used in this study are freely available through the
464 Aeris database <https://iasi.aeris-data.fr/nh3-i/> (Van Damme et al., 2021) (last access: 1 April 2022).
465 All hourly observations of PM_{2.5} concentrations are available from the Airparif network ([https://data-
466 airparif-asso.opendata.arcgis.com/](https://data-airparif-asso.opendata.arcgis.com/)), the Ministry of the Environment, Conservation and Parks of
467 Ontario (<http://www.airqualityontario.com/>), and the Red Automática de Monitoreo Atmosférico



468 (RAMA, <http://www.aire.cdmx.gob.mx/default.php?opc=%27aKBh%27>) network (last access: 1 April
469 2022). The GEOS-Chem outputs are currently available upon request. All MATLAB/PYTHON codes
470 used to create any of the figures and/or to create the underlying data are available on request.

471 **Author contributions**

472 CV, CC, SY, and KS designed the AmmonAQ project. MV and LC provided the IASI data. WP provided
473 the GEOS-Chem outputs. CV and RA analyzed the data. CV, RA, and SS wrote the manuscript draft.
474 BH, MG, KS, P-FC, and CC reviewed and edited the manuscript.

475 **Competing interests**

476 The authors declare that they have no conflict of interest.

477 **Acknowledgments**

478 AmmonAQ results from a joint research program between CNRS (National Center for Scientific
479 Research of France) and the University of Toronto which funded one year of common research in
480 2019. Research at ULB was supported by the Belgian State Federal Office for Scientific, Technical and
481 Cultural Affairs (Prodex HIRS) and the Air Liquide Foundation (TAPIR project). LC is Research
482 Associate supported by the Belgian F.R.S.-FNRS. This project has received funding from the European
483 Research Council (ERC) under the European Union's Horizon 2020 and innovation programme (grant
484 agreement No 742909, IASI-FT advanced ERC grant). The MERRA-2 data used in this study have been
485 provided by the Global Modeling and Assimilation Office (GMAO) at NASA Goddard Space Flight
486 Center.

487 **References**

488 Abeed, R., Clerbaux, C., Clarisse, L., Van Damme, M., Coheur, P.-F., Safieddine, S.: A space view of
489 agricultural and industrial changes during the Syrian civil war, *Elementa: Science of the*
490 *Anthropocene*, 9(1). doi:<https://doi.org/10.1525/elementa.2021.000041>, 2021

491 Asman, W., Sutton, M. A. and Schjörriing, J. K.: Ammonia: emission, atmospheric transport and
492 deposition, *New Phytol.*, 139, 27–48, 1998.

493 Bey, I., Jacob, D. J., Yantosca, R. M., Logan, J. A., Field, B. D., Fiore, A. M., Li, Q., Liu, H. Y., Mickley, L. J.
494 and Schultz, M. G.: Global modeling of tropospheric chemistry with assimilated meteorology: Model
495 description and evaluation, *J. Geophys. Res. Atmos.*, 106(D19), 23073–23095,
496 doi:<https://doi.org/10.1029/2001JD000807>, 2001.

497 Bouwman, A. F., Lee, D. S., Asman, W. A. H., Dentener, F. J., Van Der Hoek, K. W. and Olivier, J. G. J.: A
498 global high-resolution emission inventory for ammonia, *Global Biogeochem. Cycles*, 11(4), 561–587,
499 doi:<https://doi.org/10.1029/97GB02266>, 1997.

500 Cheng, Z., Luo, L., Wang, S., Wang, Y., Sharma, S., Shimadera, H., Wang, X., Bressi, M., de Miranda, R.
501 M., Jiang, J., Zhou, W., Fajardo, O., Yan, N. and Hao, J.: Status and characteristics of ambient PM_{2.5}
502 pollution in global megacities, *Environ. Int.*, 89–90, 212–221,
503 doi:<https://doi.org/10.1016/j.envint.2016.02.003>, 2016.



- 504 Clerbaux, C., Boynard, A., Clarisse, L., George, M., Hadji-Lazaro, J., Herbin, H., Hurtmans, D., Pommier,
505 M., Razavi, A., Turquety, S., Wespes, C. and Coheur, P.-F.: Monitoring of atmospheric composition
506 using the thermal infrared IASI/MetOp sounder, *Atmos. Chem. Phys.*, 9(16), 6041–6054,
507 doi:10.5194/acp-9-6041-2009, 2009.
- 508 Crevoisier, C., Clerbaux, C., Guidard, V., Phulpin, T., Armante, R., Barret, B., Camy-Peyret, C.,
509 Chaboureaud, J.-P., Coheur, P.-F., Crépeau, L., Dufour, G., Labonnote, L., Lavanant, L., Hadji-Lazaro, J.,
510 Herbin, H., Jacquinet-Husson, N., Payan, S., Péquignot, E., Pierangelo, C., Sellitto, P., and
511 Stubenrauch, C.: Towards IASI-New Generation (IASI-NG): impact of improved spectral resolution and
512 radiometric noise on the retrieval of thermodynamic, chemistry and climate variables, *Atmos. Meas.*
513 *Tech.*, 7, 4367–4385, <https://doi.org/10.5194/amt-7-4367-2014>, 2014.
- 514 Day, M. C., Zhang, M. and Pandis, S. N.: Evaluation of the ability of the EC tracer method to estimate
515 secondary organic carbon, *Atmos. Environ.*, 112, 317–325,
516 doi:<https://doi.org/10.1016/j.atmosenv.2015.04.044>, 2015.
- 517 Fountoukis, C. and Nenes, A.: ISORROPIA II: a computationally efficient thermodynamic equilibrium
518 model for K^+ – Ca^{2+} – Mg^{2+} – NH_4^+ – Na^+ – SO_4^{2-} – NO_3^- – Cl^- – H_2O aerosols, *Atmos. Chem. Phys.*, 7,
519 4639–4659, <https://doi.org/10.5194/acp-7-4639-2007>, 2007.
- 520 Guo, X., Wang, R., Pan, D., Zondlo, M. A., Clarisse, L., Van Damme, M., Whitburn, S., Coheur, P.-F.,
521 Clerbaux, C., Franco, B., Golston, L. M., Wendt, L., Sun, K., Tao, L., Miller, D., Mikoviny, T., Müller, M.,
522 Wisthaler, A., Tevlin, A. G., Murphy, J. G., Nowak, J. B., Roscioli, J. R., Volkamer, R., Kille, N., Neuman,
523 J. A., Eilerman, S. J., Crawford, J. H., Yacovitch, T. I., Barrick, J. D. and Scarino, A. J.: Validation of IASI
524 Satellite Ammonia Observations at the Pixel Scale Using In Situ Vertical Profiles, *J. Geophys. Res.*
525 *Atmos.*, 126(9), e2020JD033475, doi:<https://doi.org/10.1029/2020JD033475>, 2021.
- 526 Herrera B, et al.: Evolution and distribution of NH_3 over Mexico City from ground-based and satellite
527 infrared spectroscopic measurements, in prep., 2022.
- 528 Hersbach, H.; Bell, B.; Berrisford, P.; Hirahara, S.; Horányi, A.; Muñoz-Sabater, J.; Nicolas, J.; Peubey,
529 C.; Radu, R.; Schepers, D.; et al. The ERA5 global reanalysis. *Q. J. R. Meteorol. Soc.* **2020**, *146*, 1999–
530 2049, doi:10.1002/qj.3803.
- 531 Hoesly, R. M., Smith, S. J., Feng, L., Klimont, Z., Janssens-Maenhout, G., Pitkanen, T., Seibert, J. J., Vu,
532 L., Andres, R. J., Bolt, R. M., Bond, T. C., Dawidowski, L., Kholod, N., Kurokawa, J.-I., Li, M., Liu, L., Lu,
533 Z., Moura, M. C. P., O'Rourke, P. R. and Zhang, Q.: Historical (1750–2014) anthropogenic emissions of
534 reactive gases and aerosols from the Community Emissions Data System (CEDs), *Geosci. Model Dev.*,
535 11(1), 369–408, doi:10.5194/gmd-11-369-2018, 2018.
- 536 INECC and SEMARNAT 2018 México, Secretaría del Medio Ambiente de la Ciudad de México.
537 Inventario de Emisiones de la Ciudad de México 2016. Dirección General de Gestión de la Calidad del
538 Aire, Dirección de Programas de Calidad del Aire e Inventario de Emisiones. Ciudad de México.
539 Septiembre, 2018 ([http://www.aire.cdmx.gob.mx/descargas/publicaciones/flippingbook/inventario-](http://www.aire.cdmx.gob.mx/descargas/publicaciones/flippingbook/inventario-emisiones-2016/mobile/inventario-emisiones-2016.pdf)
540 [emisiones-2016/mobile/inventario-emisiones-2016.pdf](http://www.aire.cdmx.gob.mx/descargas/publicaciones/flippingbook/inventario-emisiones-2016/mobile/inventario-emisiones-2016.pdf), last access May 28 2021).



- 541 Jeong, C.-H., Traub, A., Huang, A., Hilker, N., Wang, J. M., Herod, D., Dabek-Zlotorzynska, E., Celo, V.
542 and Evans, G. J.: Long-term analysis of PM_{2.5} from 2004 to 2017 in Toronto: Composition, sources,
543 and oxidative potential, *Environ. Pollut.*, 263, 114652,
544 doi:<https://doi.org/10.1016/j.envpol.2020.114652>, 2020.
- 545 Karydis, V. A., Tsimpidi, A. P., Lei, W., Molina, L. T., and Pandis, S. N.: Formation of semi volatile
546 inorganic aerosols in the Mexico City Metropolitan Area during the MILAGRO campaign, *Atmos.*
547 *Chem. Phys.*, 11, 13305–13323, <https://doi.org/10.5194/acp-11-13305-2011>, 2011.
- 548 Larios, A. D., Chebana, F., Godbout, S., Brar, S. K., Valera, F., Palacios, J. H., Avalos Ramirez, A.,
549 Saldoval-Salas, F., Larouche, J. P., Medina-Hernández, D. and Potvin, L.: Analysis of atmospheric
550 ammonia concentration from four sites in Quebec City region over 2010–2013, *Atmos. Pollut. Res.*,
551 9(3), 476–482, doi:<https://doi.org/10.1016/j.apr.2017.11.001>, 2018.
- 552 Lee, P. K. H., Brook, J. R., Dabek-Zlotorzynska, E. and Mabury, S. A.: Identification of the Major
553 Sources Contributing to PM_{2.5} Observed in Toronto, *Environ. Sci. Technol.*, 37(21), 4831–4840,
554 doi:10.1021/es026473i, 2003.
- 555 McDuffie, E. E., Martin, R. V., Spadaro, J. V., Burnett, R., Smith, S. J., O'Rourke, P., Hammer, M. S., van
556 Donkelaar, A., Bindle, L., Shah, V., Jaeglé, L., Luo, G., Yu, F., Adeniran, J. A., Lin, J. and Brauer, M.:
557 Source sector and fuel contributions to ambient PM_{2.5} and attributable mortality across multiple
558 spatial scales, *Nat. Commun.*, 12(1), 3594, doi:10.1038/s41467-021-23853-y, 2021.
- 559 Molina, L. T., Madronich, S., Gaffney, J. S., Apel, E., de Foy, B., Fast, J., Ferrare, R., Herndon, S.,
560 Jimenez, J. L., Lamb, B., Osornio-Vargas, A. R., Russell, P., Schauer, J. J., Stevens, P. S., Volkamer, R., &
561 Zavala, M. (2010). An overview of the MILAGRO 2006 Campaign: Mexico City emissions and their
562 transport and transformation. *Atmospheric Chemistry and Physics*, 10(18), 8697–8760.
563 <https://doi.org/10.5194/acp-10-8697-2010>
- 564 Moya, M., Fountoukis, C., Nenes, A., Matías, E., and Grutter, M.: Predicting diurnal variability of fine
565 inorganic aerosols and their gas-phase precursors near downtown Mexico City, *Atmos. Chem. Phys.*
566 *Discuss.*, 7, 11257–11294, <https://doi.org/10.5194/acpd-7-11257-2007>, 2007.
- 567 Murray, C. J. L., Aravkin, A. Y., Zheng, P., Abbafati, C., Abbas, K. M., Abbasi-Kangevari, M., Abd-Allah,
568 F., Abdelalim, A., Abdollahi, M., Abdollahpour, I., Abegaz, K. H., Abolhassani, H., Aboyans, V., Abreu,
569 L. G., Abrigo, M. R. M., Abualhasan, A., Abu-Raddad, L. J., Abushouk, A. I., Adabi, M., Adekanmbi, V.,
570 Adeoye, A. M., Adetokunboh, O. O., Adham, D., Advani, S. M., Agarwal, G., Aghamir, S. M. K.,
571 Agrawal, A., Ahmad, T., Ahmadi, K., Ahmadi, M., Ahmadi, H., Ahmed, M. B., Akalu, T. Y., Akinyemi,
572 R. O., Akinyemiju, T., Akombi, B., Akunna, C. J., Alahdab, F., Al-Aly, Z., Alam, K., Alam, S., Alam, T.,
573 Alanezi, F. M., Alanzi, T. M., Alemu, B. wassihun, Alhabib, K. F., Ali, M., Ali, S., Alicandro, G., Alinia, C.,
574 Alipour, V., Alizade, H., Aljunid, S. M., Alla, F., Allebeck, P., Almasi-Hashiani, A., Al-Mekhlafi, H. M.,
575 Alonso, J., Altirkawi, K. A., Amini-Rarani, M., Amiri, F., Amugsi, D. A., Ancuceanu, R., Anderlini, D.,
576 Anderson, J. A., Andrei, C. L., Andrei, T., Angus, C., Anjomshoa, M., Ansari, F., Ansari-Moghaddam, A.,
577 Antonazzo, I. C., Antonio, C. A. T., Antony, C. M., Antriyandarti, E., Anvari, D., Anwer, R., Appiah, S. C.
578 Y., Arabloo, J., Arab-Zozani, M., Ariani, F., Armoon, B., Ärnlov, J., Arzani, A., Asadi-Aliabadi, M., Asadi-
579 Pooya, A. A., Ashbaugh, C., Assmus, M., Atafar, Z., Atnafu, D. D., Atout, M. M. W., Ausloos, F.,
580 Ausloos, M., Ayala Quintanilla, B. P., Ayano, G., Ayanore, M. A., Azari, S., Azarian, G., Azene, Z. N., et



- 581 al.: Global burden of 87 risk factors in 204 countries and territories, 1990–2019: a systematic
582 analysis for the Global Burden of Disease Study 2019, *Lancet*, 396(10258), 1223–1249,
583 doi:10.1016/S0140-6736(20)30752-2, 2020.
- 584 Nair, A. A. and Yu, F.: Quantification of Atmospheric Ammonia Concentrations: A Review of Its
585 Measurement and Modeling, *Atmosphere (Basel)*, 11(10), doi:10.3390/atmos11101092, 2020.
- 586 Ojeda-Castillo, V., Alonso-Romero, S., Mena, L. H., Álvarez-Chávez, P. E. and del Real-Olvera, J.: Air
587 Pollution in an Urban Area of Mexico: Sources of Emission (Vehicular, Natural, Industrial, and Brick
588 Production), in *Air Pollution*, edited by J. D. R. Olvera, IntechOpen, Rijeka., 2019.
- 589 Pai, S. J., Heald, C. L., Pierce, J. R., Farina, S. C., Marais, E. A., Jimenez, J. L., Campuzano-Jost, P., Nault,
590 B. A., Middlebrook, A. M., Coe, H., Shilling, J. E., Bahreini, R., Dingle, J. H. and Vu, K.: An evaluation of
591 global organic aerosol schemes using airborne observations, *Atmos. Chem. Phys.*, 20(5), 2637–2665,
592 doi:10.5194/acp-20-2637-2020, 2020.
- 593 Paulot, F. and Jacob, D. J.: Hidden Cost of U.S. Agricultural Exports: Particulate Matter from Ammonia
594 Emissions, *Environ. Sci. Technol.*, 48(2), 903–908, doi:10.1021/es4034793, 2014.
- 595 Potter, P., Ramankutty, N., Bennett, E. M., & Donner, S. D. (2010). Characterizing the Spatial Patterns
596 of Global Fertilizer Application and Manure Production. *Earth Interactions*, 14(2), 1–22.
597 <https://doi.org/10.1175/2009EI288.1>
- 598 RANDERSON, J. T., VAN DER WERF, G. R., GIGLIO, L., COLLATZ, G. J. and KASIBHATLA, P. S.: Global Fire
599 Emissions Database, Version 4.1 (GFEDv4), , doi:10.3334/ORNLDAAAC/1293, 2017.
- 600 Retama, A., Neria-Hernández, A., Jaimes-Palomera, M., Rivera-Hernández, O., Sánchez-Rodríguez, M.,
601 López-Medina, A. and Velasco, E.: Fireworks: A major source of inorganic and organic aerosols during
602 Christmas and New Year in Mexico City, *Atmos. Environ.* X, 2, 100013,
603 doi:<https://doi.org/10.1016/j.aeaoa.2019.100013>, 2019.
- 604 REYNOLDS, C. M. and WOLF, D. C.: EFFECT OF SOIL MOISTURE AND AIR RELATIVE HUMIDITY ON
605 AMMONIA VOLATILIZATION FROM SURFACE-APPLIED UREA, *Soil Sci.*, 143(2) [online] Available from:
606 [https://journals.lww.com/soilsci/Fulltext/1987/02000/EFFECT_OF_SOIL_MOISTURE_AND_AIR_RELAT](https://journals.lww.com/soilsci/Fulltext/1987/02000/EFFECT_OF_SOIL_MOISTURE_AND_AIR_RELATIVE_HUMIDITY.10.aspx)
607 [IVE_HUMIDITY.10.aspx](https://journals.lww.com/soilsci/Fulltext/1987/02000/EFFECT_OF_SOIL_MOISTURE_AND_AIR_RELATIVE_HUMIDITY.10.aspx), 1987.
- 608 Salcedo, D., Alvarez-Ospina, H., Peralta, O., & Castro, T. (2018). PM1 Chemical Characterization
609 during the ACU15 Campaign, South of Mexico City. *Atmosphere*, 9(6).
610 <https://doi.org/10.3390/atmos9060232>
- 611 Secretaría del Medio Ambiente de la Ciudad de México. Calidad del aire en la Ciudad de México,
612 Informe 2018. [Internet]. Dirección General de Calidad del Aire, Dirección de Monitoreo de Calidad
613 del Aire: Ciudad de México; 2020. Available from:
614 <http://www.aire.cdmx.gob.mx/default.php?opc=Z6Bhnml>.



- 615 Stein, A. F., Draxler, R. R., Rolph, G. D., Stunder, B. J. B., Cohen, M. D. and Ngan, F.: NOAA's HYSPLIT
616 Atmospheric Transport and Dispersion Modeling System, *Bull. Am. Meteorol. Soc.*, 96(12), 2059–
617 2077, doi:10.1175/BAMS-D-14-00110.1, 2015.
- 618 Sutton, M. A., Reis, S., Riddick, S. N., Dragosits, U., Nemitz, E., Theobald, M. R., Tang, Y. S., Braban, C.
619 F., Vieno, M., Dore, A. J., Mitchell, R. F., Wanless, S., Daunt, F., Fowler, D., Blackall, T. D., Milford, C.,
620 Flechard, C. R., Loubet, B., Massad, R., Cellier, P., Personne, E., Coheur, P. F., Clarisse, L., Van Damme,
621 M., Ngadi, Y., Clerbaux, C., Skjøth, C. A., Geels, C., Hertel, O., Wichink Kruit, R. J., Pinder, R. W., Bash,
622 J. O., Walker, J. T., Simpson, D., Horváth, L., Misselbrook, T. H., Bleeker, A., Dentener, F. and de Vries,
623 W.: Towards a climate-dependent paradigm of ammonia emission and deposition, *Philos. Trans. R.
624 Soc. Lond. B. Biol. Sci.*, 368(1621), 20130166, doi:10.1098/rstb.2013.0166, 2013.
- 625 von Bobruzki, K., Braban, C. F., Famulari, D., Jones, S. K., Blackall, T., Smith, T. E. L., Blom, M., Coe, H.,
626 Gallagher, M., Ghalaieny, M., McGillen, M. R., Percival, C. J., Whitehead, J. D., Ellis, R., Murphy, J.,
627 Mohacsi, A., Pogany, A., Junninen, H., Rantanen, S., Sutton, M. A. and Nemitz, E.: Field inter-
628 comparison of eleven atmospheric ammonia measurement techniques, *Atmos. Meas. Tech.*, 3(1),
629 91–112, doi:10.5194/amt-3-91-2010, 2010.
- 630 Van Damme, M., Clarisse, L., Franco, B., Sutton, M. A., Erisman, J. W., Wichink Kruit, R., van Zanten,
631 M., Whitburn, S., Hadji-Lazaro, J., Hurtmans, D., Clerbaux, C., & Coheur, P.-F.: Global, regional and
632 national trends of atmospheric ammonia derived from a decadal (2008–2018) satellite record.
633 *Environmental Research Letters*, 16(5), 55017. <https://doi.org/10.1088/1748-9326/abd5e0>, 2021.
- 634 Van Damme, M., Clarisse, L., Whitburn, S., Hadji-Lazaro, J., Hurtmans, D., Clerbaux, C. and Coheur, P.-
635 F.: Industrial and agricultural ammonia point sources exposed, *Nature*, 564(7734), 99–103,
636 doi:10.1038/s41586-018-0747-1, 2018.
- 637 Van Damme, M., Whitburn, S., Clarisse, L., Clerbaux, C., Hurtmans, D., and Coheur, P.-F.: Version 2 of
638 the IASI NH₃ neural network retrieval algorithm: near-real-time and reanalysed datasets, *Atmos.
639 Meas. Tech.*, 10, 4905–4914, <https://doi.org/10.5194/amt-10-4905-2017>, 2017.
- 640 Vega, E., Eidels, S., Ruiz, H., López-Veneroni, D., Sosa, G., Gonzalez, E., Watson, J. G., Edgerton, S. A.,
641 Gasca, J., Mora, V., Reyes, E., Sánchez-Reyna, G., Villaseñor, R. and Chow, J. C.: Particulate Air
642 Pollution in Mexico City: A Detailed View, *Aerosol Air Qual. Res.*, 10(3), 193–211,
643 doi:10.4209/aaqr.2009.06.0042, 2010.
- 644 Viatte, C., Petit, J.-E., Yamanouchi, S., Van Damme, M., Doucerain, C., Germain-Piaulenne, E., Gros,
645 V., Favez, O., Clarisse, L., Coheur, P.-F., Strong, K. and Clerbaux, C.: Ammonia and PM_{2.5} air pollution
646 in paris during the 2020 covid lockdown, *Atmosphere (Basel)*, 12(2), doi:10.3390/atmos12020160,
647 2021.
- 648 Viatte, C., Wang, T., Van Damme, M., Dammers, E., Meleux, F., Clarisse, L., Shephard, M. W.,
649 Whitburn, S., François Coheur, P., Cady-Pereira, K. E. and Clerbaux, C.: Atmospheric ammonia
650 variability and link with particulate matter formation: A case study over the Paris area, *Atmos. Chem.
651 Phys.*, 20(1), doi:10.5194/acp-20-577-2020, 2020.



- 652 Wang, Q., Jacob, D. J., Spackman, J. R., Perring, A. E., Schwarz, J. P., Moteki, N., Marais, E. A., Ge, C.,
653 Wang, J. and Barrett, S. R. H.: Global budget and radiative forcing of black carbon aerosol: Constraints
654 from pole-to-pole (HIPPO) observations across the Pacific, *J. Geophys. Res. Atmos.*, 119(1), 195–206,
655 doi:<https://doi.org/10.1002/2013JD020824>, 2014.
- 656 Yamanouchi, S., Viatte, C., Strong, K., Lutsch, E., Jones, D. B. A., Clerbaux, C., Van Damme, M.,
657 Clarisse, L., and Coheur, P.-F.: Multiscale observations of NH₃ around Toronto, Canada, *Atmos. Meas.*
658 *Tech.*, 14, 905–921, <https://doi.org/10.5194/amt-14-905-2021>, 2021.
- 659 Yao, X. and Zhang, L.: Causes of Large Increases in Atmospheric Ammonia in the Last Decade across
660 North America, *ACS omega*, 4(26), 22133–22142, doi:10.1021/acsomega.9b03284, 2019.
- 661 Zellweger, C., Hüglin, C., Klausen, J., Steinbacher, M., Vollmer, M., and Buchmann, B.: Inter-
662 comparison of four different carbon monoxide measurement techniques and evaluation of the long-
663 term carbon monoxide time series of Jungfraujoch, *Atmos. Chem. Phys.*, 9, 3491–3503,
664 <https://doi.org/10.5194/acp-9-3491-2009>, 2009.